Cancer Nanotechnology

RESEARCH Open Access

A [60]fullerene nanoconjugate with gemcitabine: synthesis, biophysical properties and biological evaluation for treating pancreatic cancer

Paweł Nalepa[1], Robert Gawecki[2], Grzegorz Szewczyk[3], Katarzyna Balin[2], Mateusz Dulski[4], Mieczysław Sajewicz[1], Anna Mrozek-Wilczkiewicz[2], Robert Musioł[1], Jaroslaw Polanski[1] and Maciej Serda[1*]

*Correspondence: maciej.serda@us.edu.pl
[1] Institute of Chemistry, University of Silesia in Katowice, Katowice, Poland
Full list of author information is available at the end of the article

Abstract

Background: The first-line chemotherapy drug that is used to treat pancreatic ductal adenocarcinoma is gemcitabine. Unfortunately, its effectiveness is hampered by its chemo-resistance, low vascularization and drug biodistribution limitations in the tumor microenvironment. Novel nanotherapeutics must be developed in order to improve the prognosis for patients with pancreatic cancer.

Results: We developed a synthetic methodology for obtaining a water-soluble nanoconjugate of a [60]fullerene-glycine derivative with the FDA-approved drug gemcitabine (**nanoC_{60}GEM)**. The proposed synthetic protocol enables a highly water-soluble [60]fullerene-glycine derivative **(6)** to be obtained, which was next successfully conjugated with gemcitabine using the EDCI/NHS carbodiimide protocol. The desired nanoconjugate was characterized using mass spectrometry and DLS, IR and XPS techniques. The photogeneration of singlet oxygen and the superoxide anion radical were studied by measuring $^1O_2$ near-infrared luminescence at 1270 nm, followed by spin trapping of the DMPO adducts by EPR spectroscopy. The biological assays that were performed indicate that there is an inhibition of the cell cycle in the S phase and the induction of apoptosis by nanoC_{60}GEM.

Conclusion: In this paper, we present a robust approach for synthesizing a highly water-soluble [60]fullerene nanoconjugate with gemcitabine. The performed biological assays on pancreatic cancer cell lines demonstrated cytotoxic effects of nanoC_{60}GEM, which were enhanced by the generation of reactive oxygen species after blue LED irradiation of synthesized fullerene nanomaterial.

Keywords: [60]Fullerene, Nanoconjugate, Gemcitabine, Pancreatic cancer

Background

The rapid development of nanotechnology is of great interest to researchers focused on translational medicine and novel targeted cancer treatment (Kim et al. 2010). The most popular applications of nanotherapeutics include diagnosis and treatment

of cancer, targeted drug delivery systems and in vivo imaging (Chow and Ho 2013; Dawidczyk et al. 2014). The nanotechnology approach has been used by medicinal chemists to design potential drugs that can easily break through almost any biological barrier. Engineered nanoparticles, including carbon nanomaterials, can enter tumors via their leaky vessels and remain there due to the weak drainage in the tumor microenvironment. This phenomenon is called the enhanced permeability and retention effect (*EPR effect*) and does not occur in normal tissues (Fang et al. 2011; Maeda et al. 2016). Interestingly, in our recently published article, we demonstrated that fluorescently labeled fullerenes (C_{60}-serPF) can be used as a model delivery system for biodistribution studies in a breast cancer model, due to their preferred biokinetic profile (Lapin et al. 2017a).

Since their discovery in 1985, fullerene nanomaterials have drawn the attention of medicinal chemists due to their unique biological properties (Nakamura and Isobe 2003). Over the last few decades, [60]fullerenes have been investigated for many biomedical applications, including targeted drug delivery, and as contrast agents and non-viral transfection agents (Dellinger et al. 2013). The functionalization of the fullerene cage with water solubilizing groups offers a versatile method for biological experiments, as well as for conjugation with chemotherapeutic agents, fluorescent probes and cancer-targeting antibodies (Zakharian et al. 2005; Ashcroft et al. 2006). Appropriately derivatized [60]fullerene buckyballs become amphiphilic in nature with the ability to cross most biological barriers, including the blood–brain barrier and nuclear membrane (Raoof et al. 2012). Furthermore, fullerene nanomaterials are non-toxic even at high concentrations of up to 1 mg/mL (Serda et al. 2018). The anti-cancer activity of fullerenes has mainly been described for in vivo models, where it has been explained by its ability to inhibit tumor angiogenesis (metalloproteinases inhibitors) and its strong antioxidant properties (Chen et al. 2005; Sun et al. 2016). Interestingly, it was described earlier that water-soluble fullerene derivatives have the ability to resensitize cancer cells that were previously resistant to cisplatin and doxorubicin (Zhang et al. 2009). The chemical functionalization of [60]fullerene using the cyclopropanation reaction, in which the derivatives of malonic acid are particularly useful (Bingel–Hirsch reaction), offers novel synthetic possibilities because it allows virtually any imaginable type of organic moiety to be covalently linked to the carbon shell of hydrophobic [60]fullerene.

Pancreatic cancer is a highly lethal disease that has a 5-year survival rate of less than 10% (Siegel et al. 2015). Currently, the most successful treatment is the surgical resection of the tumor, but in many cases, it is not possible to perform the surgery because only 20% of patients have resectable pancreatic cancer (Kamisawa et al. 2016). Thus, the development of non-surgical treatments, including adjuvant therapy, is needed in order to improve the prognosis for patients with pancreatic cancer. The first line of chemotherapeutic drugs that was used to treat pancreatic cancer was gemcitabine. The clinical trials that have been performed have shown that patients with advanced pancreatic cancer have better survival rates and durations after treatment with gemcitabine compared to those that were treated with 5-fluorouracil (Burris et al. 1997). Moreover, combinations of gemcitabine and different chemotherapeutic agents as well as monoclonal antibodies have also been studied for advanced breast cancer (Hu et al. 2015). Nevertheless, the usefulness of the current strategies and the effects of gemcitabine monotherapy are

hampered by its chemo-resistance, low vascularization and drug biodistribution limitations in the tumor microenvironment (Kleeff et al. 2007; Koay et al. 2014).

The use of nanoscale drugs that are designed to treat pancreatic tumors have been widely explored in the last 5 years, which has resulted in Abraxane, a nano-formulation of paclitaxel with albumin (Lee et al. 2013; Pan et al. 2015). Here, we report on a synthetic protocol that enables a water-soluble [60]fullerene nanoconjugate with gemcitabine (called **nanoC_{60}GEM**) to be generated.

Materials and methods

Materials

All of the compounds that were used were reagent grade or better, and the solvents were used as they were received unless otherwise specified. The following reagents were used as received: C_{60} (99.5%, SES RESEARCH, USA), gemcitabine (Sigma Aldrich), 2-amino-1,3-propanediol (AK Scientific), DBU (1,8-diaza-bicyclo[5.4.0]undec-7-ene, Sigma Aldrich), glycine (POCH, Poland), *p*-toluenesulfonic acid (POCH, Poland), acetic anhydride (Acros Organics), malonic acid (Acros Organics), CBr_4 (Sigma Aldrich), EDCI hydrochloride [*N*-ethyl-*N*′-(3-dimethylaminopropyl)carbodiimide hydrochloride, Acros Organics], *N*-hydroxysuccinimide (Sigma Aldrich) and sodium hydride (Acros Organics). All of the solvents that were used to prepare the carbon nanomaterials were prepared according to literature procedures by distilling them with calcium hydride and were used immediately. The nuclear magnetic resonance spectra were measured on a *Bruker Avance III 500 MHz NMR Spectrometer* with TMS as the internal standard. The MS spectra for the water-insoluble fullerenes were collected using an Autoflex II MALDI-TOF mass spectrometer, and for the water-soluble [60]fullerene derivatives using an MS electrospray ionization time-of-flight (ESI-microTOF) mass spectrometer, both instruments from Bruker Daltonics Inc (Fremont, CA, USA). The final dialysis purification of the water-soluble nanomaterial **nanoC_{60}GEM** was performed on Pall Microsep™ centrifugal membranes with molecular cut-offs 1 and 3 kDa. The purity of all of the compounds was assessed using an Agilent1260 equipped with a DAAD detector at 260 nm, RP-column: Eclipse plus C18 (3,5 μm); flow 0.5 mL/min. The Fourier transform infrared (FTIR) measurements were carried out using an Agilent Cary 640 FTIR spectrometer equipped with a standard source and a DTGS Peltier-cooled detector. The nanoconjugate powder was mixed with KBr and measured in the transmittance mode in the 700–4000 cm^{-1} range. The spectrum was recorded at 32 accumulations with a spectral resolution of 4 cm^{-1}. The obtained data were analyzed by the baseline, water, and carbon dioxide correction. The chemical analysis of the sample surface was performed using X-ray photoelectron spectroscopy (XPS). The measurements were performed on a PHI5700 Physical Electronics spectrometer. The XPS studies were carried out with using an Al Kα monochromatized X-ray source ($h\nu = 1486.6$ eV). The survey spectrum was measured at pass energy 187.75e eV, and the high-resolution core levels of C1s, F1s, N1s, O1s and Si2 were measured at pass energy 23.5 eV. The analysis of the chemical states of the detected elements, as well as the calculations of the atomic concentration was performed using MULTIPAK (version 9.6.7.1, 2015, Ulvac-phi Inc.) software. The near-infrared luminescence (1270 nm) was measured perpendicular to the excitation beam in the photon-counting mode using a thermoelectric-cooled NIR PMT

module (H10330-45; Hamamatsu, Japan) equipped with a 1100 nm cut-off filter and an additional dichroic narrow-band filter NBP, and was selectable from the spectral range 1150–1355 nm (NDC Infrared Engineering Ltd., Essex, UK). The data were collected using a computer-mounted PCI-board multichannel scaler (NanoHarp 250; PicoQuant GmbH, Berlin, Germany). Data analysis, including the first-order luminescence decay fitted using the Levenberg–Marquardt algorithm, was performed by custom-written software. The acquisition time for obtaining the singlet oxygen phosphorescence signals was 20 s. The EPR measurements were taken using a Bruker EMX-AA EPR spectrometer (Bruker BioSpin, Rheinstetten, Germany). EPR samples were run using microwave power of 10.6 mW, a modulation amplitude of 0.05 mT, center field 339.0 mT, scan width 8 mT and scan time 21 s. The light for photodynamic therapy was delivered from royal blue 100 W COB source (440 nm, FWHM 17.4 nm) (Chanzon, Shenzhen, China). The cell plate was placed in a holder above light source. Distance from the lens was set to achieve high uniformity of light power distribution on whole plate area. The cells were irradiated with 20 mW/cm^2 for 1000 s for a total dose of 20 J. Temperature of cells during irradiation did not exceed 32 °C.

Methods

Synthesis of nanoC_{60}GEM

2,2′-[(1,3-Dioxopropane-1,3-diyl)diimino]diacetic acid or malonyl-diglycine (**1**).

Glycine (9.75 g, 0.130 mol) was suspended in of 10 mL water and dissolved by adding NaOH to the solution (5.21 g, 0.130 mol). A solution of diethyl malonate in 30 mL of ethanol (10.4 g, 0.065 mol) was added and the whole mixture was placed in a 100-mL flask and heated under reflux for 3 h. The solvent was then removed on a rotary evaporator. Then, 12 M hydrochloric acid was being added to the residue until the pH of the mixture reached 1. The flask with the mixture was placed in a refrigerator for 12 h; during which the product precipitated. The resulting white solid was filtered off, washed with cold water and ethanol and dried. The final product was obtained as a white solid with a 19% yield (2.83 g) with m.p. 233 °C.

^{1}H-NMR (*d_6-DMSO, 400 MHz, ppm*): 8.35(t, J = 5.8 Hz, 2H, NH); 3.78(d, J = 5.8 Hz, 4H, CH_2–NH); 3.17 (s, 2H, –CO–CH_2–CO).

^{13}C-NMR (d_6-*DMSO, 100 MHz, ppm*): 171.5; 167.5; 42.9; 42.7; 41.2.

Diethyl 2,2′-[(1,3-dioxopropane-1,3-diyl)diimino]diacetate or diethyl malonyl-diglycinate (**2**).

Compound **1** (8.00 g, 36.67 mmol) was dissolved in 150 mL of ethanol and 348.8 mg (1.83 mmol, 5% molar ratio) of *p*-toluenesulfonic acid monohydrate was added. The reaction mixture was heated under reflux for 90 h). The solvents were then removed on a rotary evaporator to form solidifying oil. This product was purified using the extraction technique (DCM:$NaHCO_3$ solution). The organic phase was dried using anhydrous $CaCl_2$ and evaporated in vacuo to form a slightly yellowish oil. The final product was obtained with an 80% yield (8.09 g).

^{1}H-NMR (*d_6-DMSO, 500 MHz, ppm*): 8.44 (t, J = 5.7 Hz, 2H, NH);4.09 (m, 4H, CH_2–CH_3); 3.85(d, J = 5.7 Hz, 4H, CH_2–NH); 3.18(bs, 2H, –CO–CH_2–CO); 1.18(t, J = 7 Hz, 6H, CH_3).

^{13}C-NMR (*d_6-DMSO, 125 MHz, ppm*): 170.1; 167.6; 61.0; 42.9; 42.5; 41.3; 14.4, 14.3

Synthesis of diserinol malonate acetate (3)

Diserinol malonate and its peracetylated version were synthesized on a large scale using a modified protocol (Serda et al. 2018). Briefly, 2-amino-1,3-propanediol (100 g, 1076 mmol) and dimethyl malonate (57.4 mL, 500 mmol) were dissolved in dry isopropanol, heated with vigorous stirring at 50 °C for 30 min and then stirred at room temperature, under a nitrogen atmosphere for 14 days. After that time, the solid precipitate was filtered off and washed with cold isopropanol. After recrystallization from isopropyl alcohol, the white solid was obtained and dried under lyophilization (m.p. 132 °C, yield 92%). Serinol malonate (25.0 g, 99.9 mmol) was suspended in pyridine (100 mL, 1240 mmol) at 0 °C, to which acetic anhydride (150 mL, 1590 mmol) was added dropwise over the course of an hour. After reaching 25 °C, dissolution occurred and the solution was stirred continuously for 48 h. At 0 °C, methanol (50 mL, 1225 mmol) was added to quench the remaining acetic anhydride and the solution was stirred for 1 h, after which the solvents were removed in vacuo and the residue (yellow oil) was dissolved in dichloromethane and recrystallized for 12 h in hexane. The precipitate was collected as white crystals via filtration, washed with hexane and dried in vacuo (m.p. 91 °C, lit. 91–92 °C (Clark et al. 1972)).

[60]Fullerene hexakis adduct (6)

The C_{60} (360 mg, 0.500 mol) was added to a freshly distilled toluene (400 mL), mixed for 20 min using a magnetic stirrer and suspended using an ultrasonic bath. Then, CBr_4 (248.7 mg, 0.75 mmol) and malonate **2** (137.1 mg, 0.500 mmol), both of which were suspended in dichloromethane (7 mL), were added. Next, 1,8-diazabicyclo[5.4.0] undec-7-ene (DBU, 95.1 mg, 0.625 mmol) in 5 mL of DCM was added and the reaction was allowed to proceed for 3 h at room temperature. The final product was isolated using the flash chromatography technique, (silica: Mallinckrodt, 75–250 μm particles, 150 Å pore size). The unreacted residue and impurities were removed with toluene and dichloromethane and then the product was eluted with CH_2Cl_2:MeOH 5:1 (240 mL) and CH_2Cl_2:MeOH 2:1 (225 mL) mixtures. The dark brown filtrate was evaporated in vacuo to form a brown solid (powder). This final product was obtained with a 64% yield (315 mg) and the mass was confirmed using MALDI-TOF (Additional file 1: Fig. S1). The obtained monoadduct **4** (183 mg, 0.184 mmol), diserinol malonate acetate (771.1 mg, 1.843 mmol) and CBr_4 (1222.3 mg, 3.686 mmol) were dissolved in 20 mL of DCM; to which 170 mL of freshly distilled toluene was added and stirred for 5 min. Next, 1,8-diazabicyclo[5.4.0]undec-7-ene (DBU, 337 mg, 2.212 mmol) in dichloromethane (3 mL) was added slowly over the course of 4 h and the reaction was allowed to proceed with mixing at room temperature for 34 h. Flash chromatography was used (silica: Mallinckrodt, 75–250 μm particles, 150 Å pore size) to isolate the hexakis product. The unreacted residue and some of the impurities were removed with toluene and dichloromethane and then the product was eluted with a CH_2Cl_2:MeOH 5:1 (360 mL) mixture. The brown filtrate was evaporated (100 mL flask) in vacuo to form a dark brown grease (2.003 g), which was hydrolysed in order to obtain unprotected derivative **6**. For this purpose, the protected [60]fullerene derivative **5** (1.966 g) was dissolved in 20 mL of dry DCM and then sodium hydride (200.0 mg, 8.33 mmol) was carefully added in portions and stirred

for 15 min. Next, methanol was added (8 mL, in portions of 0.2–0.5 mL) and during this period, intense bubbling was observed (at the bottom of the flask, however, unreacted so it remained). The flask was tightly closed and the reaction with mixing was allowed to proceed at room temperature for 60 h. Then, 1.5 mL of methanol was added to the brown mixture in the flask; no bubbling was observed. The solvents were evaporated in vacuo to form a black solid (1.735 g). Next, a partially cleaved fullerene nanomaterial was placed in a 100-mL flask and then 1,4-dioxane (18 mL) and concentrated hydrochloric acid (3 mL, 35%) were added (the black solid product immediately dissolved). The flask was tightly closed and the reaction mixture was allowed to proceed for further hydrolysis at room temperature for 7 days. The solvents were evaporated in vacuo to form a brown solid of compound **6** (2.092 g). The final product was purified by dialysis of an aqueous solution of fullerene **6** using cellulose membranes (molecular weight exclusion limit 1.0 kDa; Spectrum Labs, USA). The dialysis lasted 7 days, and the final fullerene nanomaterial **6** was concentrated, frozen and lyophilized. The final product was obtained as a brown solid with a 35% yield (137.8 mg).

NanoC$_{60}$GEM

In a small vial, 1-ethyl-3-(3-dimethylaminopropyl)carbodiimide (EDCI, 6.60 mg, 0.034 mmol), *N*-hydroxysuccinimide (NHS, 3.96 mg, 0.034 mmol) and fullerene **6** (30.0 mg, 0.0014 mmol) were dissolved in 2 mL of a MES buffer (10% 2-(*N*-morpholino) ethanesulfonic acid in water, pH = 4.5). After 5 min of stirring, the whole mixture was added (rinsing the vial twice with 0.5 mL of the MES buffer) into a reaction vessel (10 mL) containing gemcitabine (GEM, 10.32 mg, 0.034 mmol). The [60]fullerene derivative **6** was dissolved instantly and the reaction vessel was placed on a magnetic stirrer at room temperature for 92 h. Afterwards, the final product was purified by dialysis against an aqueous solution, using a cellulose membrane (10 mL, molecular weight exclusion limit 1.0 kDa; Spectrum Labs, USA). The dialysis lasted 10 days and the water was changed twice a day. Finally, the dialysate was concentrated, frozen and lyophilized. The final product was obtained as a brown solid with a 79% yield (29.42 mg) and its purity was confirmed by HPLC (Additional file 1: Fig. S7).

Time-resolved singlet oxygen detection

Phosphate-buffered (pD 7.4, 10 mmol) D_2O solutions of nanoC$_{60}$-GEM and TMPyP in a 1-cm-optical path quartz fluorescence cuvette (QA-1000; Hellma, Mullheim, Germany) was excited by light pulses that were generated by an integrated nanosecond DSS Nd:YAG laser system, equipped with a narrow bandwidth optical parametric oscillator (NT242-1k-SH/SFG; Ekspla, Vilnius, Lithuania). The laser system delivered pulses at a 1-kHz repetition rate, with a pulse energy up to several hundred microjoules in the visible region, and up to several tens of microjoules in the UVA–UVB region. The [60] fullerene photosensitizers were photoexcited using a 427 nm wavelength. The absorbance of the samples was set to 0.27 in that wavelength. In order to adjust the photoexcitation energy in the experiments, a laser beam was attenuated with three pieces of wire mesh (light transmission 40% each). The quantum yield of singlet oxygen formation was calculated using 5,10,15,20-tetrakis(1-methyl-4-pyridinio)porphyrin tetra(*p*-toluenesulfonate) (TMPyP) as the reference compound ($\phi = 0.75$) (Snyder et al. 2006).

Electron paramagnetic resonance spin trapping studies

EPR spin trapping was used with DMPO as the spin trap at a concentration of 100 mM. Samples containing 0.1 mg/mL nanoC_{60}GEM in 80% DMSO were irradiated in EPR quartz flat cells in the resonant cavity with 402- to 508-nm (24 mW/cm^2) light, which was produced by a 300-W high-pressure compact arc xenon lamp (Cermax, PE300CE13FM/Module300W; PerkinElmer Optoelectronics, GmbH, Wiesbaden, Germany). The irradiation setup was equipped with a water filter, heat reflecting hot mirror, cut-off filter that blocked light below 390 nm and a blue additive dichroic filter 505FD64-25 (Andover Corporation, Salem, NH, USA).

Cell lines and culture methods

The human breast carcinoma; MCF-7 and human lung carcinoma epithelial-like A549 were obtained from the American Type Culture Collection (ATCC). The human pancreas adenocarcinoma AsPc-1 and pancreatic carcinoma of a ductal origin PANC-1 were obtained from Sigma-Aldrich. The murine pancreatic ductal adenocarcinoma; PAN02 was obtained from NCI-Frederick Cancer Research Facility and the normal human fibroblasts NHDF was obtained from PromoCell. The cell lines; MCF-7, A549, PANC-1 and NHDF were grown in Dulbecco's modified Eagle's medium (DMEM). The DMEM for MCF-7, A549 and PANC-1 were supplemented with 12% heat-inactivated fetal bovine serum (Sigma) and for the NHDF with 15% non-inactivated fetal bovine serum (Sigma). The AsPc-1 and PAN02 cell lines were cultured in a RPMI 1640 medium (Gibco, UK), which had been supplemented with 10% heat-inactivated fetal bovine serum (Sigma). All of the culture media were supplemented with the antibiotics penicillin/streptomycin (Gibco) (1% v/v). The cell lines were grown as monolayer cultures in 75 cm^2 flasks (Nunc) under standard conditions at 37 °C in a humidified atmosphere at 5% CO_2. All of the cell lines were tested for *Mycoplasma* contamination.

Cytotoxicity studies

The cells were seeded in 96-well plates (Nunc) at a density of 5×10^3 cells/well for the cancer cell lines and 4×10^3 cells/well for the normal cell line (NHDF) and incubated at 37 °C for 24 h. An MTS assay (CellTiter 96® AQueous One Solution Cell Proliferation Assay from Promega) was performed after a 72 h incubation of the cells using nanoC_{60}GEM (2–0.1 mg/mL) and gemcitabine (0.01–25 μM). The medium was then removed and 20 mL of a CellTiter96®AQueousOne Solution-MTS (Promega) was added to each well (with 100 mL DMEM without phenol red) and incubated at least for 1 h at 37 °C. The absorbance of the samples was measured at 490 nm using a multi-plate reader (Synergy 4, BioTek). The results which were expressed as a percentage of the control were calculated as the inhibitory concentration (IC_{50}) values using GraphPad Prism 7. Each experiment was repeated at least three times, each in triplicate.

Cell cycle assay

The PAN02 cells were seeded in 3 cm Petri dishes (Nunc) at a density of 1.5×10^5 cells/dish and incubated at 37 °C for 24 h. Then, solutions of the nanoC_{60}GEM (35

and 17 μM) and gemcitabine (1.5 and 0.75 μM) were added. After a 48-h treatment, an assay was performed using a Muse Cell-Cycle Kit (Millipore) according to the manufacturer's instructions. Briefly, the cells were collected, washed with cold PBS and centrifuged at 300*g*. Next, the cells were fixed in ice-cold 70% ethanol and stored at − 20 °C overnight. Afterwards, the cells were centrifuged and resuspended in 200 μL of a Muse™ Cell Cycle Reagent and incubated for 30 min at room temperature in the dark. After staining, the cells were processed for the cell cycle analysis using a Muse Cell Analyzer (Millipore). The experiments were performed at least three times, each in triplicate.

Annexin V binding assay

The PAN02 cells were seeded in 3-cm Petri dishes (Nunc) at a density of $1{,}5 \times 10^5$ cells/dish and incubated at 37 °C for 24 h. Then, solutions of the nanoC_{60}GEM (35 and 17 μM) and gemcitabine (1.5 and 0.75 μM) were added. After 48 h, an assay was performed using an Annexin V & Dead Cell Kit (Millipore) according to the manufacturer's instructions. Briefly, both detached and adherent cells were collected and centrifuged at 500 g for 5 min. Afterwards, the resuspended cells were incubated with 100 μL of a Muse™ Annexin V & Dead Cell Reagent for 20 min at room temperature in the dark. After staining, the events for live, early and late apoptotic cells were counted using a Muse Cell Analyzer (Millipore). The experiments were performed at least three times, each in triplicate.

Photodynamic therapy on the PAN02 cell line

The PAN02 line cells were plated in 24-well plates at density of 35,000/well. Twenty-four hours after plating, the cells were incubated with high-glucose DMEM that contained nanoC_{60}GEM at different concentrations. Feeding was repeated two more times, at 24-h intervals. The day after the final feeding the cells were washed twice with PBS that contained calcium and magnesium ions, then irradiated for 15 min using a blue led light (440 nm) at a fluence rate 20 mW/cm^2. Dark control cells were kept in the same conditions except light exposure. After irradiation, the cells were provided with DMEM with 10% FBS. The cytotoxic effect of the photodynamic treatment was quantified 24 h after irradiation, using a MTT assay for the mitochondrial redox function. The MTT solution in DMEM with 10% FBS was added to the treated and control culture wells (final concentration of 0.5 mg/mL). After incubation for 30 min at 37 °C, the culture medium was removed and the remaining blue precipitate was solubilized in DMSO, followed by reading the absorbance at 560 nm in a plate reader (GENios Plus, Tecan Austria GmbH). The results are reported as the percentage of the paired untreated controls. The experiments were repeated a minimum of three times.

Statistical analysis

The results are expressed as the mean ± standard deviation (SD) from at least three independent experiments. A statistical analysis was performed using the one-way ANOVA with a Bonferroni post hoc test. A p value of 0.05 or less was considered to be statistically significant. GraphPad Prism v.7.0 software (GraphPad Software, USA) was used for the analysis (Fig. 1).

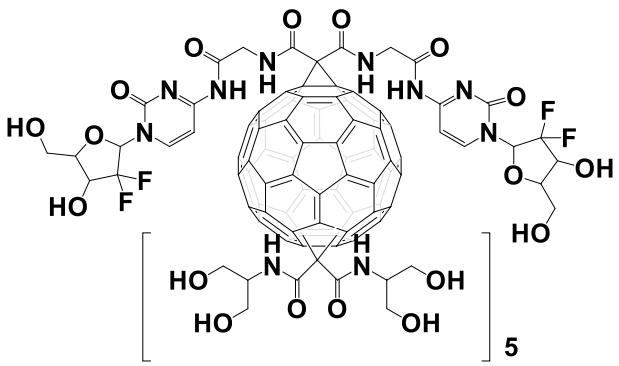

Fig. 1 Chemical structure of nanoC_{60}-GEM

Results and discussion

Synthetic protocol and characterization of nanoC_{60}GEM

The synthetic protocol for obtaining nanoC_{60}GEM is shown in Scheme 1. During our design step, we decided to use a glycine derivative of malonic acid **1** as the substrate for the Bingel–Hirsch reaction. We expected that the carboxylic groups, which are present in that compound would be much more reactive toward the aromatic amines (i.e., the cytosine fragment in the gemcitabine) in contrast to the malonic acid derivatives, which are closely connected the [60]fullerene scaffold, based on literature findings (Wang et al. 2015). The desired [60]fullerene monoadduct **4** was created in a high yield by in situ generation of α-brominated malonate **2** in the presence of CBr_4/DBU at room temperature in a time-controlled reaction, where monoadducts were formed up to 3 h. However, after that time, bis- and tris-adducts formed, which made the purification process more complicated. The structure of the monoadduct **4** was confirmed using MALDI-TOF spectrometry with a characteristic peak at 992 Da and no presence of the bis- or tris-adducts (Additional file 1: Fig. S1). The second Bingel–Hirsh reaction was performed using diserinol malonate acetate (malonate **3**) in order to ensure a high degree of water solubility and the desired hexakis adduct with T_h symmetry was created (compound **5**) in a good yield. The deprotection of fullerene **5** was performed in a two-step procedure, which involved hydrogenolysis with sodium hydride first and then the final hydrolysis with 1,4-dioxane with concentrated HCl added. The molecular peak of the [60]fullerene derivative **6** is shown in Additional file 1: Fig. S2 with the characteristic mass of 2195 Da $[M+H_2O+H]^+$ and no signals from the pentakis isomer. The final step of the conjugation with GEM was performed using the water-soluble carbodiimide EDCI/NHS system in a solution of a MES buffer. The ESI spectrometry confirmed the formation of the desired nanoC_{60}GEM (Additional file 1: Fig. S3) which had a characteristic signal of the molecular peak at 2690 Da $[M+Na]^+$, which represented the [60]fullerene derivative **6** that had been conjugated to two molecules of gemcitabine via an amide bond. Interestingly, a fragmentation pattern, in which one serinol group left the nanoC_{60}GEM (characteristic at 2578 Da, Additional file 1: Fig. S3), was observed.

The UV–VIS spectrum of nanoC_{60}GEM is characteristic for the water-soluble fullerenes that have a high absorbance only in the UV and blue regions of a spectrum (max absorbance was observed at 220 nm). Moreover, we found that nanoC_{60}GEM tends to form monodisperse aggregates around 120 nm as was confirmed by DLS (Additional

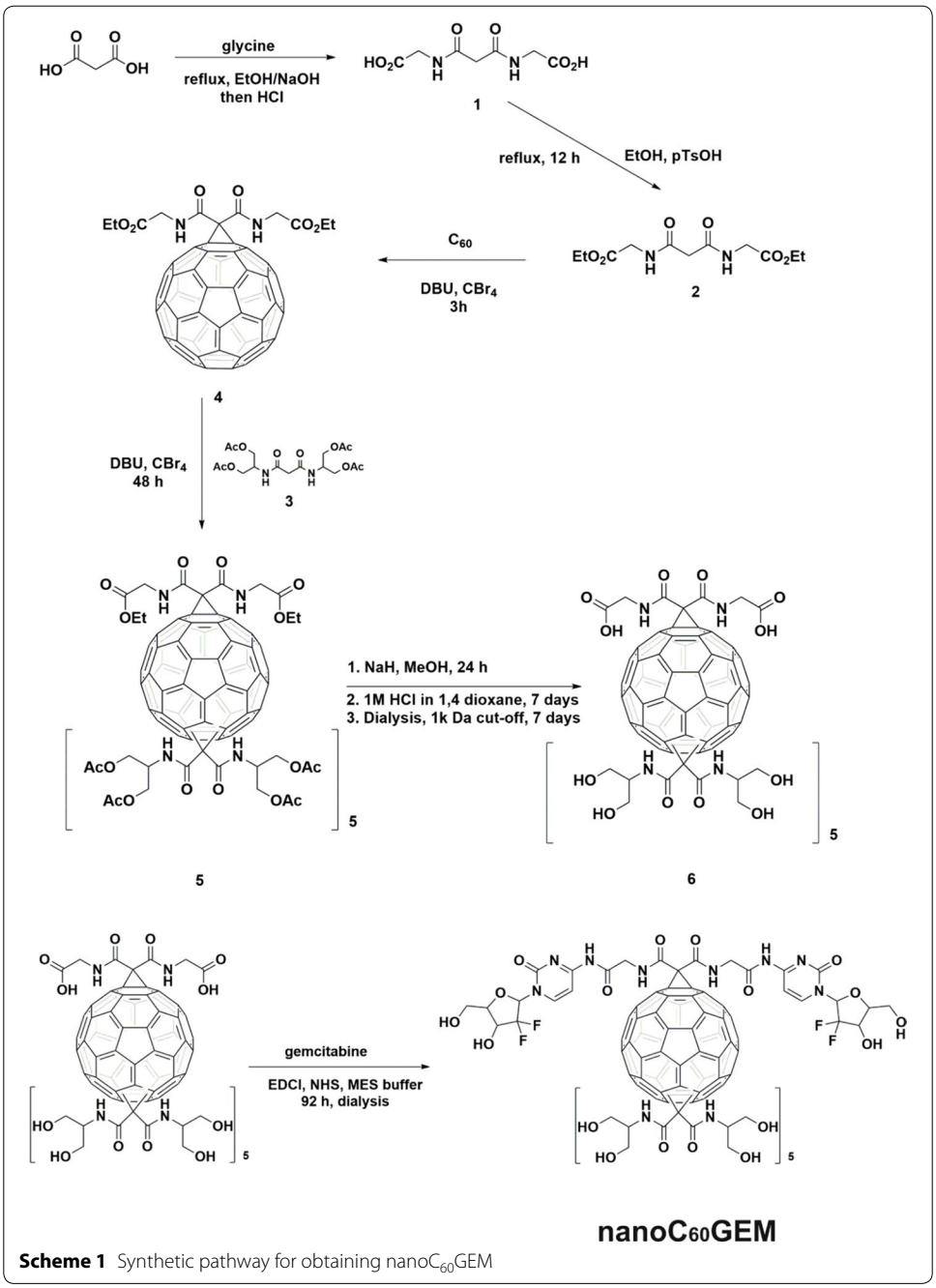

Scheme 1 Synthetic pathway for obtaining nanoC_{60}GEM

file 1: Fig. S4), and which may be disintegrated into smaller individual fullerenes inside the cell (Lapin et al. 2017b). The zeta potential measurements of our gemcitabine nanoconjugate (Additional file 1: Fig. S5) also indicated a surface charge of − 25 mV, thus confirming a relatively good degree of stability.

The infrared spectrum of the nanoC_{60}GEM system was divided into two spectral regions: (1) 2700–3800 cm^{-1} and (2) 700–1850 cm^{-1} (Fig. 2). The high wavenumber region is characterized by the presence of a broadened band that is centered at 3364 cm^{-1}, which corresponded to the overlapping signal that had originated from the

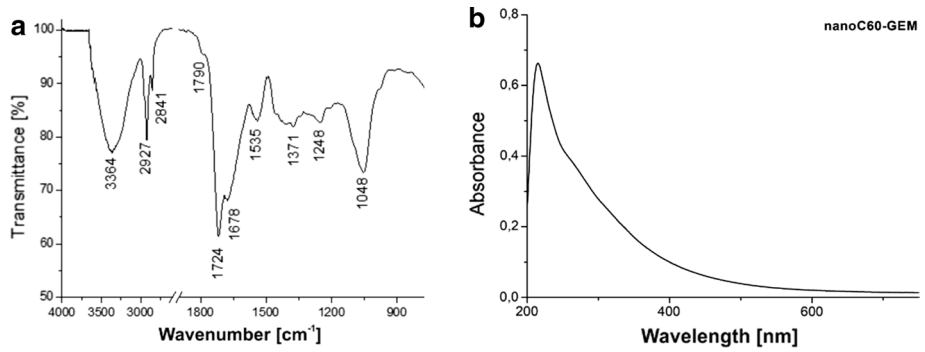

Fig. 2 **a** Infrared spectrum of nanoconjugate measured in the 700–4000 cm^{-1} range. **b** UV–VIS spectrum of nanoC_{60}GEM recorded in ultrapure water ($c = 0.01$ mg/mL)

hydroxyl (Motoyama and Jarboe 1966) and the secondary amide vibration (Lumley Jones 1963). The observable band shift toward a lower wavenumber, especially in relation to the hydroxyl group, may have resulted from the formation of an inter- or intramolecular hydrogen bonding scheme. In turn, the low-wavenumber bands with their maxima centered at 2927 and 2841 cm^{-1} may have originated from the asymmetric and symmetric stretching mode of the methylene groups that overlapped with the stretching vibration of the CH moieties.

The fingerprint (1) region, especially at high wavenumbers with a maxima located at 1790, 1724 and 1678 cm^{-1}, is determined by the carbonyl stretching modes due to primary amides (Craig and Evans 1965). The deformational mode of the secondary amide could have corresponded to the band at 1535 cm^{-1}. In addition, this band has a combination character with vibration originated from the medium–strong vibration within the furan (Katritzky and Lagowski 1959) as well as the C=C and C=N ring stretching vibrations within the pyrimidin-2-one (Billes et al. 1998). The other low-intense bands with their maxima at 1371 and 1248 cm^{-1} were mainly linked to the deformational modes of the methylene groups that were located within the aliphatic chain or the furan and pyrimidin-2-one rings. In turn, the interpretation of the band at 1048 cm^{-1} was unambiguous because of the overlapping character of the various modes that may be activated at this wavenumber such as a C=C–H deformation within the aliphatic moieties or within the furan and pyrimidin-2-one, the CN of a secondary amine or asymmetric and symmetric vibration of the CF. In turn, the deformational mode of the CF could have been expected at 726 cm^{-1}. Finally, one can summarize that the band arrangement indicated on the presence of the hydroxyl, secondary amine, and fluorine substituents, which confirmed that the synthesis had been performed successfully.

The chemical states of the elements that were present on a sample surface were analyzed using XPS. The change in the binding energy was related to changes in the chemical bonding with the surrounding elements. An analysis of the carbon chemical states was performed to analyze the C1s core level. A resolved line, see Fig. 3a, indicates the presence of several different chemical states of the carbon. The state with the lowest binding energy of 282.84 eV was associated with the presence of an impurity of an SiC origin. The amount of this state was relatively low about 4.19% of the entire amount of carbon (see Additional file 1: Table S1). The highest peak, which

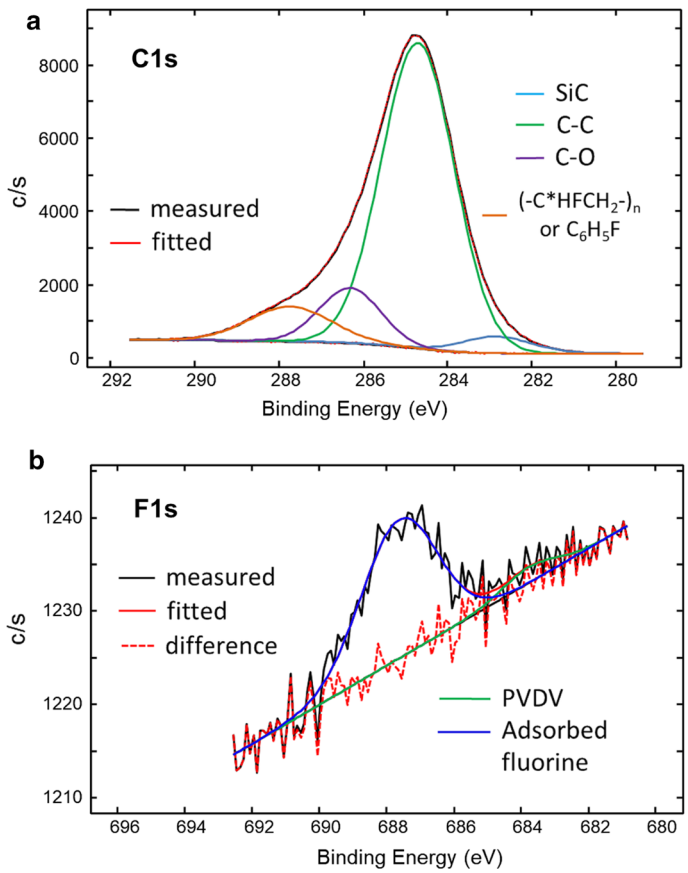

Fig. 3 The XPS high-resolution photoemission lines of nanoC_{60}-GEM: **a** carbon C1s, and **b** fluorine F1s

was located at 284.71 eV, indicates the presence of C–C and C–H type bonds (Watts 1993). The peak centered at 286.33 eV could be assigned to the C–O and C–N bonds and has been the case for other fullerene derivatives (Yu et al. 2012), whereas the peak at 287.74 eV corresponds to the states that have been observed in poly(vinyl fluoride) (Clark et al. 1973) or fluorobenzene (Clark et al. 1972) compounds. Fluorine analysis was difficult, mainly due to the quality of the spectrum, which resulted from the small amount of this element in the sample. Calculations of the atomic concentration indicated about 0.06 atomic percent of F on the sample surface, which is generally the detection limit of the XPS technique.

Nevertheless the fluorine 1s photoemission line had (see Fig. 3b) a peak that was located at 687.63 eV, and similar values were observed for graphite fluorides for which the peaks located in the range of 687–689 eV were assigned to the adsorbed fluorine (Palchan et al. 1989). The weakly developed peak at 687.63 eV may be associated with polyvinylidene fluoride (PVDF); however, as this state represents only 7% of all of the fluorine, which is itself a trace element, the analysis could not be precise. An analysis of oxygen confirmed what had been observed in the C1s C–O bonds. For nitrogen, the N1s line indicated the presence of two chemical states, one weakly developed at 397.57 eV, which was related to the Si_3N_4 compound and the second of high intensity

at 399.78 eV, which was related to the bonds that present in nylon. In the case of silicone, two chemical states were also present, one was centered at 100.33 eV and was related to SiC and the second at 102.02 eV, which was related to Si_3N_4. Additionally, a small amount of bromine was observed and was associated with AgBr. Taking into account the atomic concentrations, which were calculated from the XPS measurements, in which the amount of carbon was approximately 79.39 at.%, oxygen 15.36 at.%, nitrogen 3.89 at.%, fluorine 0.06 at.%, silicone 1.14 at.%, and bromine 0.15 at.%, both the Si and Br can be treated as trace elements that appeared due to synthetic impurities or sample preparation.

Biophysical characterization of nanoC_{60}GEM

The water-soluble [60]fullerene nanomaterials are well-known for their ability to produce different types of reactive oxygen species when irradiated by blue light (Mroz et al. 2007).

Based on previous literature studies, in polar solvents, in particular those containing donor electrons such as NADH, the irradiation of fullerenes leads to the generation of reduced oxygen species, such as superoxide anion radical ($O_2^{\bullet -}$) and hydroxyl radical (OH•). In non-polar solvents such as benzene, the process of singlet oxygen ($^1O_2$) is primarily formed (Yamakoshi et al. 2003). UV light has a very low ability to penetrate through tissue and can cause a non-specific effect in any cells it hits. In our study, we used blue LED light, which has a slightly better tissue penetration that does not cause any damage to cells that have no photosensitizer. The photoreactivity of the analyzed fullerene nanoparticles was determined by measuring their ability to generate, after irradiation with blue LED light, singlet oxygen and superoxide anion, which may have oxidizing effects on several cellular targets, especially under conditions with a low-oxygen concentration. In this study, we carried out singlet oxygen photogeneration studies of nanoC_{60}GEM using a cationic porphyrin (TMPyP) as the reference photosensitizer.

The calculated quantum efficiency of $^1O_2$ formation for our water-soluble [60]fullerene derivative, which had been irradiated by blue LED light was around 0.05. Although the efficacy of singlet oxygen formation for pristine fullerene is almost at unity (at 532 nm), chemical modifications can decrease their efficacy (Arbogast et al. 1991). Earlier studies with Bingel–Hirsch products confirmed the observation that monoadducts as well as aminofullerenes produce singlet oxygen more effectively than hexakis adducts (as nanoC_{60}GEM) (Hamblin 2018). More importantly, we discovered that in the presence of bovine serum albumin (100 mM) this process is reduced, suggesting a close interaction between fullerene and the formation of the protein corona (Fig. 4c).

We also measured superoxide photogeneration using the EPR spin-trapping method with DMPO as the spin trap. While nanoC_{60}GEM alone showed a negligible signal of trapped adducts, the presence of electron donor (NADH) increased the signal by an order of magnitude (Fig. 4b), thus showing that in favorable conditions, the electron transfer route may also contribute to a phototoxic effect. Spin trapping was performed in 80% DMSO, which made any measurements in the presence of BSA impossible as it would have destroyed the protein structure. Although the photoreactivity of our novel fullerene nanomaterial is not very high, its localization within cancer cells could make it more phototoxic if it is localized, for example, in the nucleus (Serda et al. 2018).

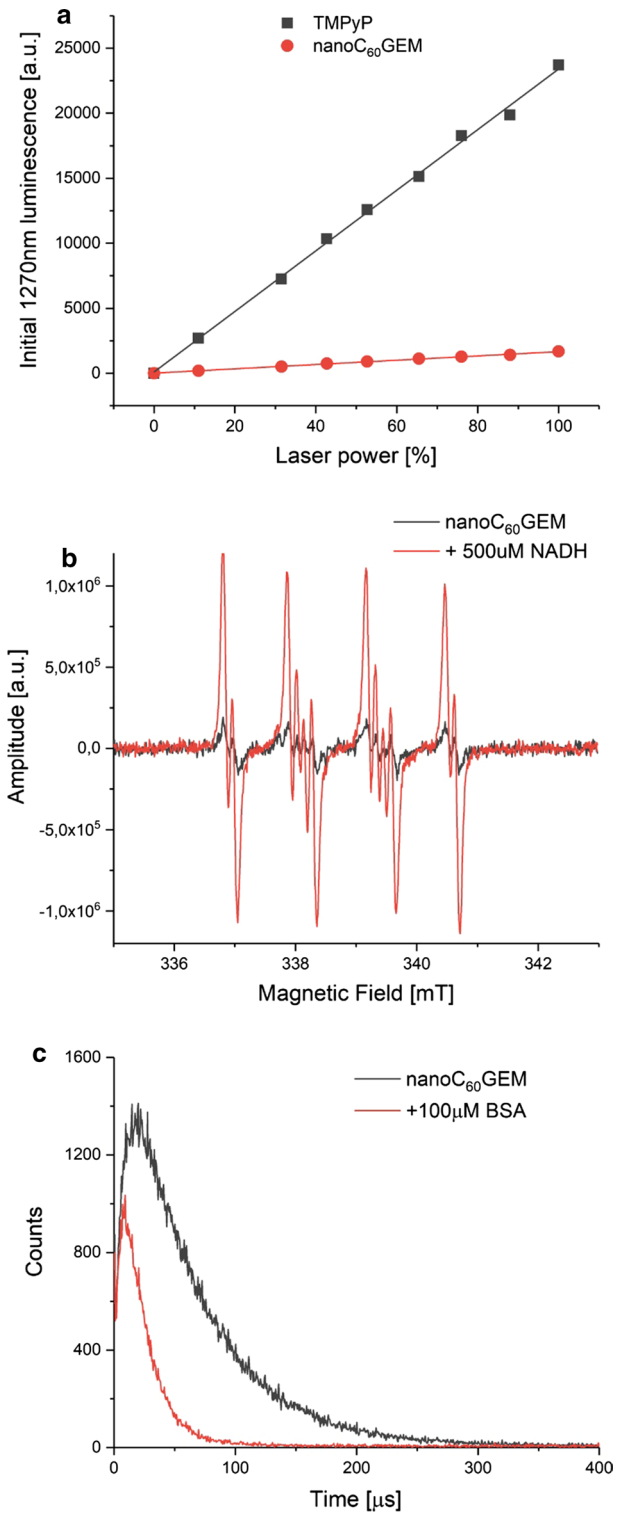

Fig. 4 Photoreactivity of nanoC_{60}GEM. **a** Quantum yield of singlet oxygen generation after irradiation by blue LED light by nanoC_{60}GEM with TMPyP used as the reference photosensitizer; **b** spin adduct signal (DMPO-OOH) that was formed in the absence and presence of an electron donor (0.5 mM NADH) after blue LED light irradiation; **c** 1270 nm luminescence observed in the absence and presence (100 μM) of bovine serum albumin

Biology

Cytotoxicity

We performed cytotoxicity screening using several cancer cell lines of different origins including normal human fibroblasts. During the biological studies, we decided to study pancreatic, breast and lung cancers because of the clinical use of GEM for the aforementioned neoplasms (Xie et al. 2018; Watanabe et al. 2019). The calculated IC_{50} values are presented in Table 1.

We observed a noticeable cytotoxicity for two cell lines, MCF-7 and PAN02, for which we calculated the IC_{50} parameters to be 2.07 ± 0.64 and 7.35 ± 1.13 μM, respectively. Compared to gemcitabine alone, the cytotoxic effect was reduced. A possible explanation of this phenomenon may be the ineffective transport of nanoC_{60}GEM into the nucleus. Gemcitabine is a deoxycytidine analog with two additional fluoride atoms and as nucleoside derivative, it is transported throughout human nucleoside transporters (hNTs) (Mackey et al. 1998).

We hypothesized that after GEM was conjugated with [60]fullerene, this type of transport would be unavailable. Additionally, GEM is incorporated into the C60 structure by the formation of an amide bond which, for steric hindrance, is probably difficult to access through the cellular enzymes such as proteases. Despite its higher activity toward the MCF-7 cell line, we selected the PAN02 cell line for the further studies because we also wanted to perform in vivo studies.

Cell cycle

In order to evaluate the mechanism of action of nanoC_{60}GEM, we performed a flow cytometry measurement. As is presented in Fig. 5, after 48 h of the incubation with nanoC_{60}GEM and gemcitabine, we observed a decrease in the faction of cells in the G0/G1 phase (compared to the control). However, there was an increase in the number of cells in the S phase in all of the cases that were examined regardless of the concentration. This increase indicated an inhibition of the cell cycle in the S phase. This is consistent with Huang's studies for gemcitabine (Huang et al. 1991), which indicates that it inhibits DNA synthesis. After its uptake into a cell, gemcitabine is metabolized into an active triphosphate form. Thereafter, this form is embedded in the DNA chain, thereby preventing its elongation.

Cell death

In order to determinate the type of the cell death, we also used flow cytometry. In this experiment, after 48 h of incubation with nanoC_{60}GEM and gemcitabine, we measured the green signal that was derived from apoptotic cells. As is presented in Fig. 6, the

Table 1 Antiproliferative activity of the studied compounds

Compound	IC_{50} [μM]					
	MCF-7	AsPc-1	PAN02	PANC-1	A549	NHDF
NanoC_{60}GEM	2.07 ± 0.64	> 375	7.35 ± 1.13	> 375	> 375	> 375
Gemcitabine	0.044 ± 0.008	0.207 ± 0.046	0.027 ± 0.003	21.95 ± 3.99	> 25	> 25

The IC_{50} parameters were calculated using GraphPad Prism 7

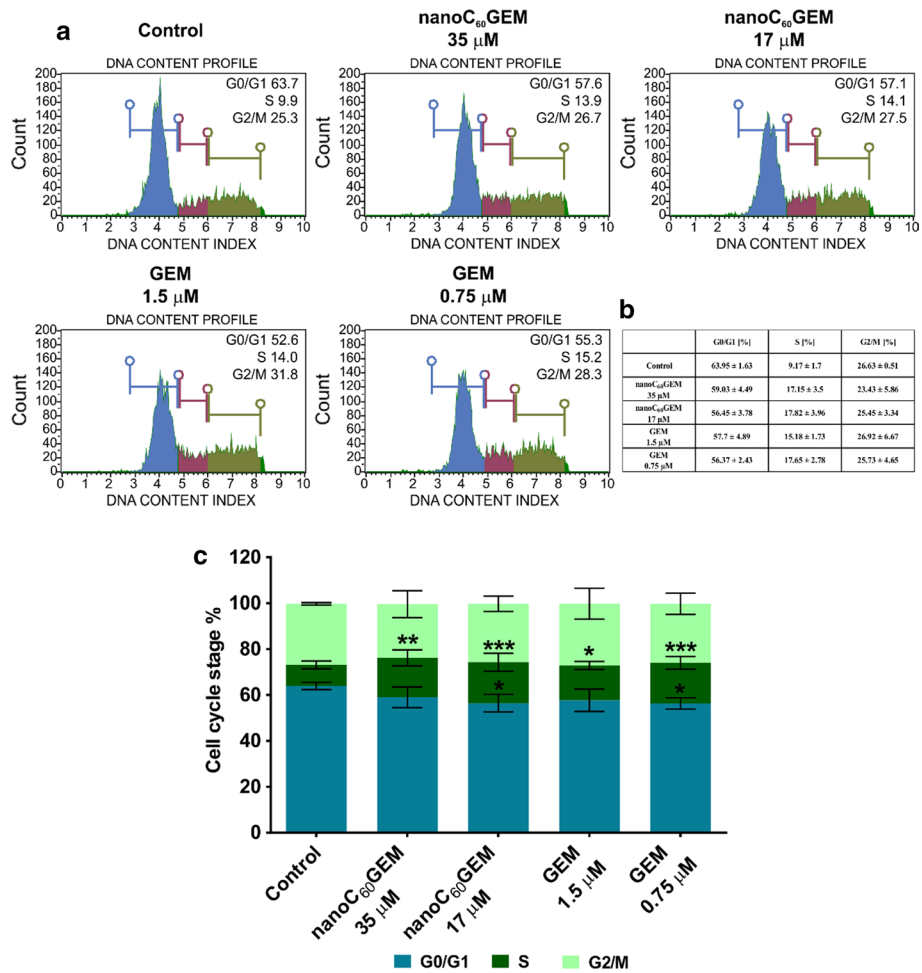

	G0/G1 [%]	S [%]	G2/M [%]
Control	63.95 ± 1.63	9.17 ± 1.7	26.63 ± 0.51
$nanoC_{60}$GEM 35 μM	59.03 ± 4.49	17.15 ± 3.5	23.43 ± 5.86
$nanoC_{60}$GEM 17 μM	56.45 ± 3.78	17.82 ± 3.96	25.45 ± 3.34
GEM 1.5 μM	57.7 ± 4.89	15.18 ± 1.73	26.92 ± 6.67
GEM 0.75 μM	56.37 ± 2.43	17.65 ± 2.78	25.73 ± 4.65

Fig. 5 Effect of the tested $nanoC_{60}$GEM (35 and 17 μM) and GEM (1.5 and 0.75 μM) on regulating the cell cycle in the PAN02 cell line. The histograms show the distribution of the cells in the G0/G1, S and G2/M phases of the cell cycle for an exemplary experiment (**a**). The table shows the mean ± SD percentage of the cells in the G0/G1, S and G2/M phases of the cell cycle from three independent experiments (**b**). The data were analyzed using a one-way ANOVA with a Bonferroni's post hoc test: $^{*}p < 0.05$, $^{**}p < 0.01$, $^{***}p < 0.001$ compared to the control (**c**)

biggest fraction of the apoptotic cell was detected for gemcitabine (44% compared to the control). There was no big difference between the two concentrations of GEM (0.75 and 1.5 μM) that were tested. However, for $nanoC_{60}$GEM, we also registered a comparable population of apoptotic cells (38.6% for 35 μM of $nanoC_{60}$GEM). These results are promising from the perspective of further studies.

Phototoxicity studies

According to research reports, [60]fullerene derivatives have a great potential to be used as photosensitizers in photodynamic therapy. In order to evaluate this hypothesis, we performed experiments in which the cells were incubated with $nanoC_{60}$GEM for 3 days to cause the cellular nucleases to cleave GEM from the nanoconjugate, after which the cells were irradiated with blue LED light. After the

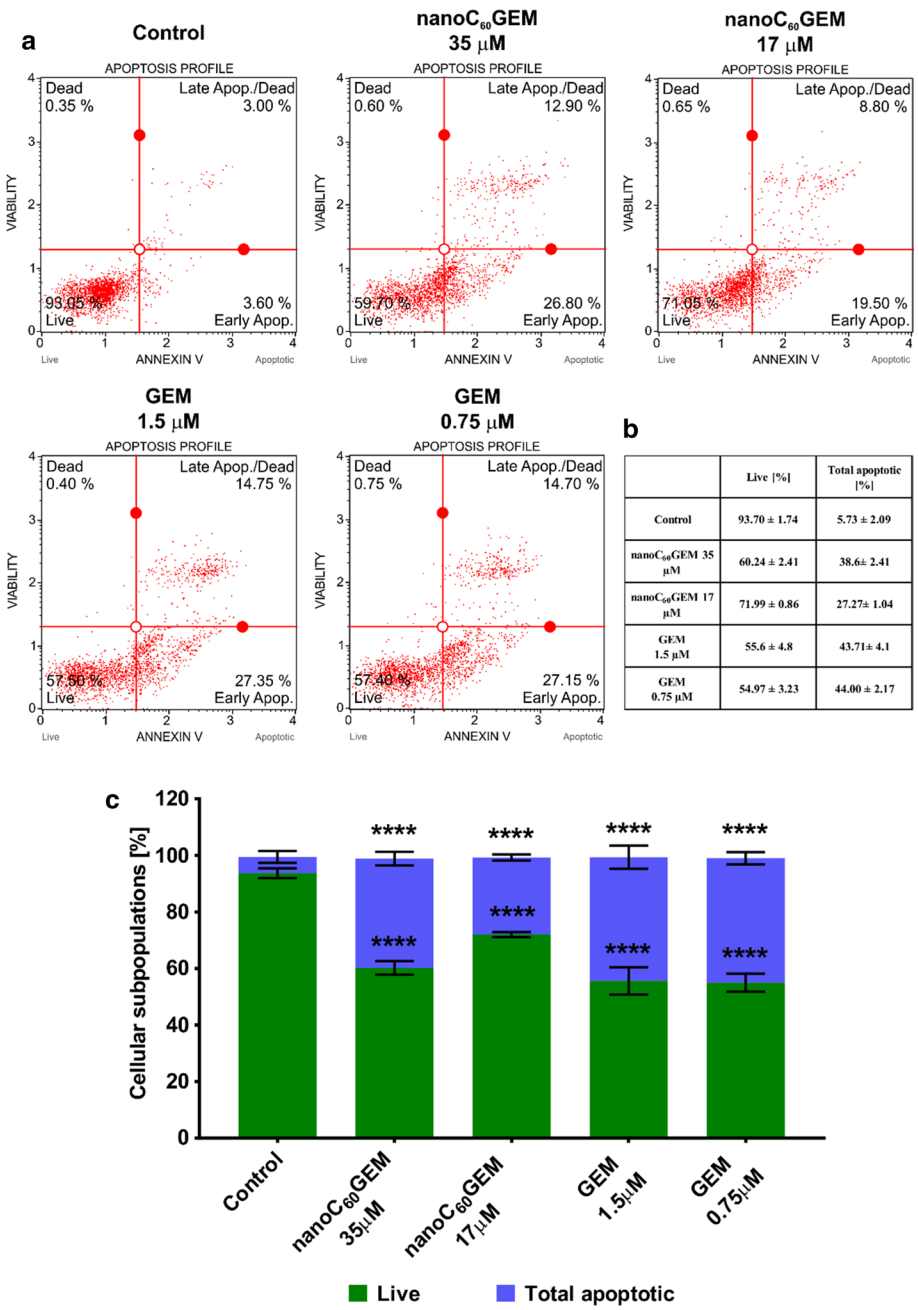

Fig. 6 Evaluation of the induction of apoptosis in the PAN02 cell line after a 48-h treatment with nanoC$_{60}$GEM (35 and 17 μM) and GEM (1.5 and 0.75 μM). The histograms show the percentage of early and late apoptosis for one of the experiments (**a**). The table shows the mean ± SD percentage of the live, early and late apoptotic cells from three independent experiments (**b**). The data were analyzed using one-way ANOVA with a Bonferroni's post hoc test: *$p < 0.05$, **$p < 0.01$, ***$p < 0.001$ compared to the control (**c**)

irradiation a cell viability assay was performed (24 h, MTT). The selection of the correct wavelength (440 nm) to be used was dictated by the absorption properties of the studied nanomaterial (Fig. 2b), in order to avoid UV part of the spectrum that could cause unspecific effects. As is depicted in Additional file 1: Fig. S4, the tested

compound did not generate a significant level of the singlet oxygen and superoxide anion. Addition of an electron donor increased the superoxide production many-fold (Fig. 4b), but such favorable conditions are difficult to find in a cellular environment. Therefore, we conducted the experiments by adding BSA (Fig. 4c), which confirmed the interaction of the fullerene nanomaterial and the formation of the protein corona. Our results show that the interaction with conducts serum protein leads to a decrease in the observable signal of singlet oxygen, which may be caused by a decreased yield of the generation or by an increased quenching of the singlet oxygen by bounded proteins. To explore this issue in depth, we performed in vitro studies using a medium that contained FBS. The results, which are presented in Fig. 7, confirmed the non-toxic properties of the low concentrations of irradiated nanoC_{60}GEM, which reduced the chances of using this type of fullerene nanomaterial as a photosensitizer. Although the PAN02 cell line phototoxicity response was disappointing, we plan to study the effects of nanoC_{60}GEM on different cancer cell lines and 3D-spheroids.

Conclusions

The developed synthetic protocol was able to produce a highly water-soluble [60]fullerene nanoconjugate with gemcitabine in good yield. The physio-chemical characteristics of the fullerene nanomaterial confirms that two gemcitabine units are attached to the [60]fullerene scaffold via formation of amide bonds. The nanoC_{60}GEM cytotoxicity effect was dependent on its concentration in PAN02 cells, but its phototoxic effects were mild, partly due to the formation of the protein corona on the surface of the [60]fullerene scaffold as well as the low quantum yields of the singlet oxygen generation. Further biological studies using 3D-spheroids as well as murine models should be used in order to evaluate the efficacy of a therapy using nanoC_{60}GEM.

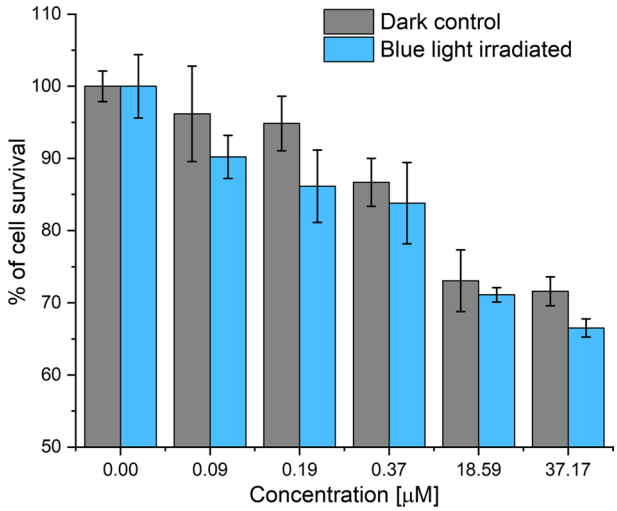

Fig. 7 Phototoxicity of nanoC_{60}GEM performed for the PAN02 cancer cell line

Supplementary information

Supplementary information accompanies this paper at https://doi.org/10.1186/s12645-020-00058-4.

Additional file 1. The physico-chemical characteristics of nanocC_{60}GEM.

Abbreviations

ATCC: American Type Culture Collection; BSA: Bovine serum albumin; DLS: Dynamic light scattering; DMEM: Dulbecco's modified Eagle medium; DBU: 1,8-Diaza-bicyclo[5.4.0]undec-7-ene; DCM: Dichloromethane; DMPO: 5,5-Dimethyl-1-pyrroline *N*-oxide; DMSO: Dimethylsulfoxide; DNA: Deoxyribonucleic acid; EDCI: 1-Ethyl-3-(3-dimethylamino propyl) carbodiimide; EPR: Enhanced permeability and retention effect; EPR: Electron paramagnetic resonance; FBS: Fetal bovine serum; FDA: Food and Drug Administration; GEM: Gemcitabine; IC_{50}: Half-maximal inhibitory concentration; LED: Light emitting diode; MALDI: Matrix-assisted laser desorption/ionization; μM: Micromolar; MS: Mass spectrometry; MTT: (3–[4,5–Dimethyl-thiazol-2-yl]-2,5-diphenyltetrazolium bromide); NADH: Nicotinamide adenine dinucleotide reduced form; nanoC_{60}GEM: [60]Fullerene derivative nanoconjugate with gemcitabine; NHS: *N*-Hydroxysuccinimide; PBS: Phosphate-buffered saline; PVDF: Polyvinylidene fluoride; RPMI: Roswell Park Memorial Institute; S phase: Synthesis phase; TMPyP: 5,10,15,20-Tetrakis(1-methyl-4-pyridinio)porphyrin tetra(*p*-toluenesulfonate); XPS: X-ray photoelectron spectroscopy.

Acknowledgements

Not applicable.

Authors' contributions

Conception and design: MS, GSZ and AMW. Acquisition of data: PN, RG, GS, MS, KB, MD, and MS. Analysis and interpretation of the data: MS, GSZ and AMW. Manuscript preparation: MS, GSZ, AMW, JP and RM wrote the manuscript. All authors read and approved the final manuscript.

Funding

Dr. Maciej Serda thanks the National Science Center (Poland) for its support (Grant SONATA UMO-2016/23/D/NZ7/00912). Dr. Mateusz Dulski is thankful for the financial support from the National Science Center based on decision 2017/26/D/ST8/01117.

Availability of data and materials

The datasets used and/or analyzed during the current study are available from the corresponding author on reasonable request.

Ethics approval and consent to participate

Not applicable.

Consent for publication

Not applicable.

Competing interests

We confirm that we have given due consideration to the protection of intellectual property associated with this work and that there are no impediments to publication, including the timing of publication, with respect to intellectual property. The authors declare that they have no competing interests.

Author details

[1] Institute of Chemistry, University of Silesia in Katowice, Katowice, Poland. [2] Institute of Physics and Silesian Center for Education and Interdisciplinary Research, University of Silesia in Katowice, Katowice, Poland. [3] Faculty of Biochemistry, Biophysics and Biotechnology, Jagiellonian University, Kraków, Poland. [4] Institute of Materials Engineering and Silesian Center for Education and Interdisciplinary Research, University of Silesia in Katowice, Katowice, Poland.

Received: 5 October 2019 Accepted: 3 February 2020
Published online: 18 February 2020

References

Arbogast JW, Darmanyan AP, Foote CS, Diederich FN, Whetten RL, Rubin Y, Alvarez MM, Anz SJ. Photophysical properties of sixty atom carbon molecule (C60). J Phys Chem. 1991;95(1):11–2.

Ashcroft JM, Tsyboulski DA, Hartman KB, Zakharian TY, Marks JW, Weisman RB, Rosenblum MG, Wilson LJ. Fullerene (C60) immunoconjugates: interaction of water-soluble C60 derivatives with the murine anti-gp240 melanoma antibody. Chem Commun. 2006;28:3004–6.

Billes F, Mikosch H, Holly S. A comparative study on the vibrational spectroscopy of pyridazine, pyrimidine and pyrazine. J Mol Struct (Thoechem). 1998;423(3):225–34.

Burris HA 3rd, Moore MJ, Andersen J, Green MR, Rothenberg ML, Modiano MR, Cripps MC, Portenoy RK, Storniolo AM, Tarassoff P, et al. Improvements in survival and clinical benefit with gemcitabine as first-line therapy for patients with advanced pancreas cancer: a randomized trial. J Clin Oncol. 1997;15(6):2403–13.

Chen C, Xing G, Wang J, Zhao Y, Li B, Tang J, Jia G, Wang T, Sun J, Xing L, et al. Multihydroxylated [Gd@C82(OH)22]n nanoparticles: antineoplastic activity of high efficiency and low toxicity. Nano Lett. 2005;5(10):2050–7.

Chow EK, Ho D. Cancer nanomedicine: from drug delivery to imaging. Sci Transl Med. 2013;5(216):216rv214.

Clark DT, Kilcast D, Adams DB, Musgrave WKR. An ESCA study of the molecular core binding energies of the fluorobenzenes. J Electron Spectrosc Relat Phenom. 1972;1(3):227–50.
Clark D, Feast W, Kilcast D, Musgrave W. Applications of ESCA to polymer chemistry. III. Structures and bonding in homopolymers of ethylene and the fluoroethylenes and determination of the compositions of fluoro copolymers. J Polym Sci. 1973;11(2):389–411.
Craig NC, Evans DA. Infrared and Raman Spectra of cis- and trans-1,2-dichloro-1,2-difluoroethylene. J Am Chem Soc. 1965;87(19):4223–30.
Dawidczyk CM, Kim C, Park JH, Russell LM, Lee KH, Pomper MG, Searson PC. State-of-the-art in design rules for drug delivery platforms: lessons learned from FDA-approved nanomedicines. J Control Release. 2014;187:133–44.
Dellinger A, Zhou Z, Connor J, Madhankumar AB, Pamujula S, Sayes CM, Kepley CL. Application of fullerenes in nanomedicine: an update. Nanomedicine. 2013;8(7):1191–208.
Fang J, Nakamura H, Maeda H. The EPR effect: unique features of tumor blood vessels for drug delivery, factors involved, and limitations and augmentation of the effect. Adv Drug Deliv Rev. 2011;63(3):136–51.
Hamblin MR. Fullerenes as photosensitizers in photodynamic therapy: pros and cons. Photochem Photobiol Sci. 2018;17(11):1515–33.
Hu X-C, Zhang J, Xu B-H, Cai L, Ragaz J, Wang Z-H, Wang B-Y, Teng Y-E, Tong Z-S, Pan Y-Y, et al. Cisplatin plus gemcitabine versus paclitaxel plus gemcitabine as first-line therapy for metastatic triple-negative breast cancer (CBCSG006): a randomised, open-label, multicentre, phase 3 trial. Lancet Oncol. 2015;16(4):436–46.
Huang P, Chubb S, Hertel LW, Grindey GB, Plunkett W. Action of 2′, 2′-difluorodeoxycytidine on DNA synthesis. Cancer Res. 1991;51(22):6110–7.
Kamisawa T, Wood LD, Itoi T, Takaori K. Pancreatic cancer. Lancet. 2016;388(10039):73–85.
Katritzky A, Lagowski J: 130. Infrared absorption of heteroaromatic, five-membered, monocyclic nuclei. Part I. 2-Monosubstituted furans. *Journal of the Chemical Society (Resumed)* 1959:657-660.
Kim BY, Rutka JT, Chan WC. Nanomedicine. N Engl J Med. 2010;363(25):2434–43.
Kleeff J, Beckhove P, Esposito I, Herzig S, Huber PE, Lohr JM, Friess H. Pancreatic cancer microenvironment. Int J Cancer. 2007;121(4):699–705.
Koay EJ, Baio FE, Ondari A, Truty MJ, Cristini V, Thomas RM, Chen R, Chatterjee D, Kang Y, Zhang J, et al. Intra-tumoral heterogeneity of gemcitabine delivery and mass transport in human pancreatic cancer. Phys Biol. 2014;11(6):065002.
Lapin NA, Krzykawska-Serda M, Dilliard S, Mackeyev Y, Serda M, Wilson LJ, Curley SA, Corr SJ. The effects of non-invasive radiofrequency electric field hyperthermia on biotransport and biodistribution of fluorescent [60]fullerene derivative in a murine orthotopic model of breast adenocarcinoma. J Control Release. 2017a;260:92–9.
Lapin NA, Vergara LA, Mackeyev Y, Newton JM, Dilliard SA, Wilson LJ, Curley SA, Serda RE. Biotransport kinetics and intratumoral biodistribution of malonodiserinolamide-derivatized [60]fullerene in a murine model of breast adenocarcinoma. Int J Nanomed. 2017b;12:8289–307.
Lee GY, Qian WP, Wang L, Wang YA, Staley CA, Satpathy M, Nie S, Mao H, Yang L. Theranostic nanoparticles with controlled release of gemcitabine for targeted therapy and MRI of pancreatic cancer. ACS Nano. 2013;7(3):2078–89.
Lumley Jones R. The infrared spectra of some simple N-substituted amides in the vapor state. J Mol Spectrosc. 1963;11(1):411–21.
Mackey JR, Mani RS, Selner M, Mowles D, Young JD, Belt JA, Crawford CR, Cass CE. Functional nucleoside transporters are required for gemcitabine influx and manifestation of toxicity in cancer cell lines. Cancer Res. 1998;58(19):4349–57.
Maeda H, Tsukigawa K, Fang J. A retrospective 30 years after discovery of the enhanced permeability and retention effect of solid tumors: next-generation chemotherapeutics and photodynamic therapy—problems, solutions, and prospects. Microcirculation. 2016;23(3):173–82.
Motoyama I, Jarboe CH. Hydroxyl Group Stretching Frequency and Extinction Coefficient Studies on Aliphatic Alcohols. The Journal of Physical Chemistry. 1966;70(10):3226–8.
Mroz P, Pawlak A, Satti M, Lee H, Wharton T, Gali H, Sarna T, Hamblin MR. Functionalized fullerenes mediate photodynamic killing of cancer cells: type I versus Type II photochemical mechanism. Free Radical Biol Med. 2007;43(5):711–9.
Nakamura E, Isobe H. Functionalized fullerenes in water. the first 10 years of their chemistry, biology, and nanoscience. Acc Chem Res. 2003;36(11):807–15.
Palchan I, Crespin M, Estrade-Szwarckopf H, Rousseau B. Graphite fluorides: an XPS study of a new type of C-F bonding. Chem Phys Lett. 1989;157(4):321–7.
Pan Y, Wang L, Kang SG, Lu Y, Yang Z, Huynh T, Chen C, Zhou R, Guo M, Zhao Y. Gd-metallofullerenol nanomaterial suppresses pancreatic cancer metastasis by inhibiting the interaction of histone deacetylase 1 and metastasis-associated protein 1. ACS Nano. 2015;9(7):6826–36.
Raoof M, Mackeyev Y, Cheney MA, Wilson LJ, Curley SA. Internalization of C60 fullerenes into cancer cells with accumulation in the nucleus via the nuclear pore complex. Biomaterials. 2012;33(10):2952–60.
Serda M, Ware MJ, Newton JM, Sachdeva S, Krzykawska-Serda M, Nguyen L, Law J, Anderson AO, Curley SA, Wilson LJ, et al. Development of photoactive Sweet-C60 for pancreatic cancer stellate cell therapy. Nanomedicine (Lond). 2018;13(23):2981–93.
Siegel RL, Miller KD, Jemal A. Cancer statistics, 2015. CA Cancer J Clin. 2015;65(1):5–29.
Snyder JW, Lambert JD, Ogilby PR. 5, 10, 15, 20-tetrakis (N-Methyl-4-Pyridyl)-21 H, 23H-porphine (TMPyP) as a sensitizer for singlet oxygen imaging in cells: characterizing the irradiation-dependent behavior of TMPyP in a single cell. Photochem Photobiol. 2006;82(1):177–84.
Sun C, Wang L, Gao D, Pan Y, Zhao Y, Chen C, Guo M. C60(OH)22: a potential histone deacetylase inhibitor with antiangiogenic activity. Nanoscale. 2016;8(36):16332–9.
Wang L, Zhu X, Tang X, Wu C, Zhou Z, Sun C, Deng S-L, Ai H, Gao J. A multiple gadolinium complex decorated fullerene as a highly sensitive T 1 contrast agent. Chem Commun. 2015;51(21):4390–3.
Watanabe S, Yoshioka H, Sakai H, Hotta K, Takenoyama M, Yamada K, Sugawara S, Takiguchi Y, Hosomi Y, Tomii K. Necitumumab plus gemcitabine and cisplatin versus gemcitabine and cisplatin alone as first-line treatment for stage IV squamous non-small cell lung cancer: a phase 1b and randomized, open-label, multicenter, phase 2 trial in Japan. Lung Cancer. 2019;129:55–62.

Watts JF. High resolution XPS of organic polymers: the Scienta ESCA 300 database. G. Beamson and D. Briggs. 280 pp.,£ 65. John Wiley & Sons, Chichester, ISBN 0471 935921,(1992). Surf Interface Anal. 1993;20(3):267.
Xie Z, Zhang Y, Jin C, Fu D. Gemcitabine-based chemotherapy as a viable option for treatment of advanced breast cancer patients: a meta-analysis and literature review. Oncotarget. 2018;9(6):7148.
Yamakoshi Y, Umezawa N, Ryu A, Arakane K, Miyata N, Goda Y, Masumizu T, Nagano T. Active oxygen species generated from photoexcited fullerene (C60) as potential medicines: O2-• versus 1O2. J Am Chem Soc. 2003;125(42):12803–9.
Yu J, Guan M, Li F, Zhang Z, Wang C, Shu C, Wei H, Zhang X-E. Effects of fullerene derivatives on bioluminescence and application for protease detection. Chem Commun. 2012;48(89):11011–3.
Zakharian TY, Seryshev A, Sitharaman B, Gilbert BE, Knight V, Wilson LJ. A fullerene — paclitaxel chemotherapeutic: synthesis, characterization, and study of biological activity in tissue culture. J Am Chem Soc. 2005;127(36):12508–9.
Zhang Q, Yang W, Man N, Zheng F, Shen Y, Sun K, Li Y, Wen L-P. Autophagy-mediated chemosensitization in cancer cells by fullerene C60 nanocrystal. Autophagy. 2009;5(8):1107–17.

Publisher's Note